I. Nesteruk

Institute of Hydromechanics, National Academy of Sciences of Ukraine, Kyiv, Ukraine
NTUU "Igor Sikorsky Kyiv Polytechnic Institute", Kyiv, Ukraine

EFFICIENCY OF STEADY MOTION AND ITS IMPROVEMENT WITH THE USE
OF UNSEPARATED AND SUPERCAVITATING FLOW PATTERNS

Background. The efficiency of the steady subsonic motion of vehicles and animals in air and water is estimated with the use of different drag coefficients, the drag-to-weight and power-to-weight ratios.

Objective. The improvement of these characteristics with the use of special shaped hulls and wing profiles which remove boundary layer separation and with the use of the supercavitating flow pattern for the high-speed motion in water.

Methods. Analytical and numerical estimations with the use of known results for flow on slender unseparated body of revolution and airfoil and for the steady supercavitating flow pattern.

Results. Simple analytic formulae were obtained for the movement efficiency, the critical Reynolds numbers of the laminar-to-turbulent transition etc. and applied for different terrestrial, aquatic and airborne vehicles, animals and human sport activity. In a rather large range of the Reynolds number $10^6 \le \mathrm{Re}_V \le 10^8$, the use of unseparated shapes yields very substantial reduction of the drag in comparison with the conventional bodies of revolution. In water at $\mathrm{Re}_V > 10^7$ the supercavitating flow pattern can be preferable.

Conclusions. This drag reduction opens up prospects for designing different kinds of very effective airborne and high-speed underwater vehicles.

Keywords: unseparated shapes; drag reduction; laminar-to-turbulent transition; supercavitation; drag-to-weight ratio; power-to-weight ratio.

Introduction

Modern technologies open new horizons for vehicles allowing substantially increase their speed as well as to increase or to reduce their size. For example, researchers in China are reporting that they have taken a big step towards creating a supersonic submarine. This technology could theoretically get from Shanghai to San Francisco − about 6,000 miles − in just 100 minutes [1]. On the other hand, the dimensions of modern vehicles vary in a very wide range. For example, the length of oil tankers can exceed 400 meters while a remote control Nano Quad Copter from Revell measures only 45 mm square, [2].

Different shapes of vehicles and flow patterns are used to diminish the drag and to improve the efficiency. For steady motion in water or in air, it is very important to reduce negative effects of the boundary layer separation, since the separation zones increase the pressure drag and noise. To remove separation active and passive boundary-layer control methods are used. Here we concentrate on the passive flow control methods, which use only the shaping of the rigid-body in order to ensure negative pressure gradients over almost the entire body and thus prevent flow separation. These methods do not use any additional energy supply to remove separation in comparison with the active methods such as suction/blowing, surface cooling/ heating or different shape transformations. During last 20 years the possibility of achieving an attached flow on a rigid body has been investigated in the Institute of Hydromechanics (IHM) of National Academy of Sciences, Kyiv, Ukraine. The survey of these theoretical and experimental studies is presented in [3]. The developed and tested unseparated bodies of revolution are rather similar to the shapes of fast aquatic animals, e.g., dolphins [4].

The drag of underwater vehicles can be reduced by decreasing the area wetted by water, i.e., by the use of supercavitation (see, e.g., [5, 6]). In the case of supercavitation the main part of the hull is located inside the cavity, therefore the skin-friction drag can be significantly reduced, since the density of vapor or/and gas inside the cavity is approximately 800 time less than the water density. This idea was developed in many theoretical, numerical and experimental investigations in many countries. In particular, the supersonic velocities (greater than the speed of sound $a \approx 1450$ m/s) were achieved for small supercavitating projectiles, launched by guns or special catapults [5].

In this paper we evaluate the effectiveness of the movement in air and water with the use of such criteria as drag coefficients, drag-to-weight and power-to-weight ratios. We will estimate these characteristics in order to answer very important questions:

1. When the vehicle hulls without boundary-layer separation (see, e.g., [3, 4]) are preferable in comparison with conventional shapes?

2. When the supercavitation (see, e.g., [5, 6]) must be used for high-speed underwater vehicles?

3. In which cases the neutral buoyant vehicles are preferable in air and water?

4. Is it possible to have fully laminar vehicles and what is their effectiveness?

We will compare the motion effectiveness of vehicles, animals and the human sport activities.

Problem formulation

Development and application of simple efficiency criteria for the steady subsonic motion of vehicles and animals in air and water.

Materials and Methods

Drag coefficients. The drag $X = X_W + X_U$ for the steady horizontal motion can be divided into parts. The first one

$$X_W = \frac{mg(1-\alpha)}{k_W}, \quad \alpha = \frac{\rho V}{m} \qquad (1)$$

is connected with the supporting of the vehicle weight *mg*. The buoyancy coefficient α expresses the difference in the density of air or water ρ and the average vehicle density ($\alpha = 1$ for neutral buoyant vehicles or animals, e.g., ships, airships or fish); k_W is usually constant (e.g., aerodynamic efficiency for airplanes), $1/k_W$ is a friction coefficient for cars, trains or bikes. The air- or hydrodynamic drag X_U depends on the velocity *U* and can be expressed with the use of different drag coefficients, based on the vehicle volume *V*, different areas *A*, e.g., frontal, wetted or the cavitator base area ($A = \pi R_n^2$) and on the depth of an underwater movement *h* (in meters):

$$X_U = 0.5 C_V \rho U^2 V^{2/3}$$
$$= C_{Vh}\rho g(h+10)V^{2/3} = 0.5C_x\rho U^2 A. \qquad (2)$$

For example, hydro- or aerodynamical drag coefficient C_{xS} of slender bodies of revolution can be calculated with the use of semi-empiric Hoerner formulas [7]. For a purely laminar boundary layer:

$$C_{xS} = C_{fl}[1 + 1.5(D/L)^{1.5}] + 0.11(D/L)^2 \qquad (3)$$

where

$$C_{fl} = \frac{1.328}{\sqrt{\mathrm{Re}_L}}, \quad \mathrm{Re}_L = \frac{UL}{\nu} \qquad (4)$$

are the flat-plate skin-friction coefficient and the Reynolds number (see, e.g., [8]). For a purely turbulent boundary layer

$$C_{xS} = C_{ft}[1 + 1.5(D/L)^{1.5} + 7(D/L)^3] \qquad (5)$$

where

$$C_{ft} = \frac{0.0307}{\mathrm{Re}_L^{1/7}} \qquad (6)$$

is the flat-plate skin-friction coefficient (see, e.g., [8]). C_{xS} is based on the wetted area *S*; *D* and *L* are the maximum body diameter and its length; ν is the kinematic viscosity of water or air.

In the case of supercavitation, created by disc or non-slender conic cavitators (with the angle 2θ, $\theta > 25^0$, see Fig. 1, *b*) at subsonic velocities, the semi-empiric Garabedian formulas [9] were used in [10, 11] to calculate the volumetric drag coefficient for a vehicle which uses the cavity volume completely (as shown in Fig. 1, *b*):

$$C_V = \sqrt[3]{\frac{9\pi\sigma^4}{-16\ln\sigma}}, \quad \sigma = \frac{2g(h+10)}{U^2} \qquad (7)$$

where σ is the cavitation number (pressure of vapor and gas inside the cavity is neglected). It must be noted that the value C_V does not depend on θ and tends to zero with diminishing of the cavitation number (or with increasing the velocity).
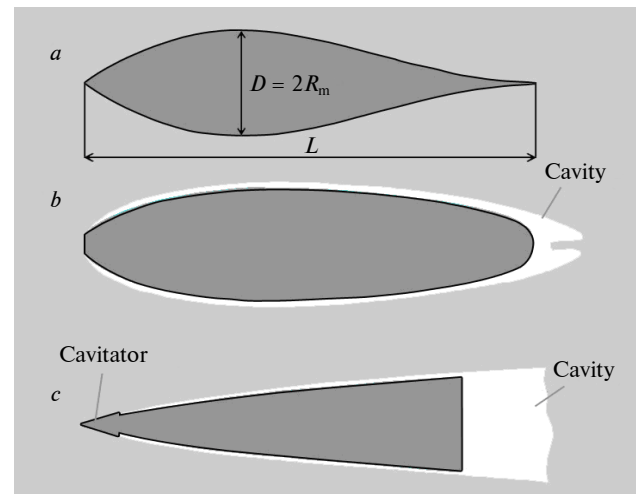

Fig. 1. Different axisymmetric flow patterns: *a* − flow without boundary layer separation (in the air or in the water); *b* − supercavitation in water with a disc cavitator; *c* − supercavitation in water with a slender conical cavitator; the hull is located in the nose part of the cavity only
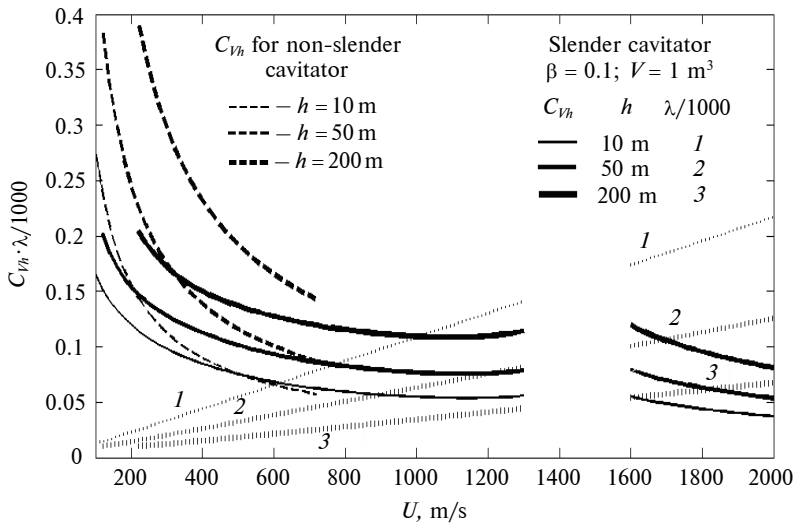
Fig. 2. Drag coefficients C_{Vh} and the cavitator + cavity aspect ratio $\lambda = L/D$ at different values of the depth $h = 10; 50; 200$ m [6]. C_{Vh} for disc and non-slender conical cavitators, eq. (7) — dashed lines; for the slender conical cavitator, $\beta = \text{tg}(\theta) = 0.1$; $V = 1$ m^3 — solid lines. Values $\lambda / 1000$ for the slender conical cavitator, $\beta = 0.1$ — dotted lines

For slender conical cavitators, the radius $R(x)$ of the axisymmetric cavity and the pressure drag of the slender conical cavitator can be estimated with the use of slender body theory [12−14]. The corresponding drag coefficients C_V and C_{Vh} were calculated in [6], see Fig. 2.

Fig. 2 demonstrates a very surprising fact that the drag of a supercavitating vehicle of a fixed volume (its hull shape is changeable to be located inside the cavity), moving at constant depth, decreases with the increasing the velocity. In particular, the drag of a proper shaped supersonic vehicle can be smaller than subsonic one. This feature is only inherent supercavitation. In air (or in water without separation) the drag drastically increases with speed. To estimate the drag of the high-speed subsonic supercavitating vehicle with the slender cavitator at a moderate depth of movement, the following approximation can be used, see Fig. 2:

$$C_{Vh} \approx 0.1. \qquad (8)$$

Diminishing the drag coefficients is important in order to increase to speed of vehicle, since at given power, the velocity will be maximum at the minimal value of the drag coefficient.

Drag-to-weight and drag-to-lift ratios. The commercial efficiency of vehicles can be estimated with the use of drag-weight ratio $1/k$. The minimal value of this parameter yields the maximum of tons×kilometers which can be transported by the vehicle per unit of time, [15]. With the fixed fuel

(or another energy) capacity on its board, a vehicle with the maximum value of k has the maximum range. With the use of (1), (2) this efficiency criterion may be expressed as follows:

$$\frac{1}{k} = \frac{1-\alpha}{k_W} + \frac{C_V \rho\, U^2 V^{2/3}}{2mg}$$

$$= \frac{1-\alpha}{k_W} + 0.5\alpha\, C_V\, \text{Fr}_V^2 , \qquad (9)$$

and is related to the volumetric Froude number:

$$Fr_V^2 = \frac{U^2}{gV^{1/3}} = \frac{\text{Fr}_L^2 L}{V^{1/3}}. \qquad (10)$$

The drag-to-weight ratio can also be treated as the cost of motion, i.e. how much energy is used to move 1N of weight to the distance of 1m. Usually in literature, this characteristic is related to the 1 kg of mass or weight — $Jkg^{-1}m^{-1}$ (see, e.g., [16]). By dividing the values in $Jkg^{-1}m^{-1}$ by 9.8 (the value of gravity constant), we obtain the dimensionless criterion, coinciding with (9).

If the wigs support the weight of the vehicle, the lift-to-weight ratio (the aerodynamic efficiency) must be maximum ($k_W \rightarrow$ max in formula (9)). The limited aspect ratio of wing $\lambda_W = b/H$ (b is span, H is the average chord length) causes so known inductive drag, which is equal to the friction one at the maximum value of the aerodynamic efficiency, (see, e.g., [8]):

$$k_{\max} = 0.5\sqrt{\frac{\pi \varepsilon b^2}{C_f S_{\text{wet}}}} \qquad (11)$$

where S_{wet} is the wetted area of the wing, $\varepsilon \leq 1$ is the coefficient corresponding to the circulation distribution on the wing (usually is close to unit), C_f is the friction coefficient (e.g., (4) or (6)).

Power-to-weight ratio and capacity-efficiency. To estimate the maneuverability of the vehicle, e.g., its ability to increase the velocity, the power-to-weight ratio is used. Since for the steady motion the mechanical power used for propulsion is the product of drag and velocity, the power-to-weight ratio can be written as follows (see (9)):

$$P_W = \frac{U}{k} = \frac{U(1-\alpha)}{k_W} + 0.5\alpha\, U C_V\, Fr_V^2. \qquad (12)$$

The total power of vehicle engines (or released in an animal's body) significantly exceeds the estimation (12) which takes into account only the part of the power converted into propulsion. Thus, P_W can be rewritten as the product of the total available power per unit weight q and the propulsion efficiency η $(0 < \eta < 1)$. The drag cannot be measured in many cases (especially on animals). Nevertheless, it is possible to obtain an estimation of the efficiency by using the minimal possible value of the drag coefficient corresponding to the laminar unseparated flow in (12).

The drag on the slender unseparated body of revolution was estimated in [17] with the use of the Mangler–Stepanov transformations and Blasius solution for the flat plate boundary layer (see, e.g., [8]) and the following simple formula was obtained:

$$C_V = \frac{4.7}{\sqrt{\mathrm{Re}_V}}; \quad \mathrm{Re}_V = \frac{UV^{1/3}}{\nu}. \tag{13}$$

Eq. (13) shows that the volumetric frictional drag coefficient C_V does not depend on the slender body shape, provided its volume remains constant, and is a reliable estimate for the minimum possible drag on a rigid body of revolution (see also [4]).

Substitution (13) into (12) yields a new characteristic — capacity-efficiency:

$$C_E = (P_W)_{\min} = (q\eta)_{\min} = \frac{U(1-\alpha)}{k_W}$$

$$+2.35\frac{U^{2.5}\alpha\sqrt{\nu}}{g\sqrt{V}} = \frac{U(1-\alpha)}{k_W} + 2.35\frac{U^{2.5}\sqrt{\alpha\rho\nu}}{g\sqrt{m}}. \tag{14}$$

For the neutral buoyant body $(\alpha = 1)$ formula (14) yields:

$$C_E = 2.35\frac{U^{2.5}\sqrt{\nu}}{g\sqrt{V}} = 2.35\frac{U^{2.5}\sqrt{\rho\nu}}{g\sqrt{m}}. \tag{15}$$

Equation (15) allows comparison the efficiency of different animals and vehicles with the information about their velocity and mass (or volume) only. Some results are presented in [4].

It must be noted that it is impossible to increase the power-to-weight ratio (or the capacity-efficiency) and to decrease the drag-to-weight ratio simultaneously, since these characteristics are related by simple equation $kP_W = U$. Thus, for a given velocity increasing of maneuverability P_W (or C_E) causes the decreasing of the commercial efficiency k.

Theoretical estimations

Drag and lift force on slender unseparated shapes. When the boundary layer separates from a body surface, the boundary layer thickness and the pressure drag increase. Separation causes recirculating fluid motion, and usually induces vortices and turbulence in the flow and hence tends to an increase of noise and to a decrease the lift force on wings. Thus, shapes without separation are of obvious interest, since they allow one to reduce both drag and noise and to increase the lift on wings.

Many investigations have been carried out with the use of active flow control methods in order to avoid separation and to delay the laminar-to-turbulent transition (see, e.g., [18–20]). These active control methods are usually based on suction/blowing, surface cooling/heating, different shape transformations and even electromagnetic forces. Proper use of these methods can delay the transition to the turbulent flow pattern and reduce or even remove flow separation, but all of them need additional energy to be supplied.

In comparison, passive flow control methods use only the shaping of the rigid-body and its surface properties. This means that no external energy has to be added to perform the control. Here we concentrate on special body shaping in order to ensure negative pressure gradients over almost the entire body and thus to prevent flow separation. During last 20 years the possibility of achieving an attached flow on a rigid body has been investigated in the Institute of Hydromechanics of National Academy of Sciences, Kyiv, Ukraine. The survey of these theoretical and experimental studies is presented in [3]. An example – shape UA-2c – is shown in Fig. 1, *a*. Wind tunnel tests revealed the absence of separation on some of proposed bodies of revolution at large Reynolds number range, in particular on the unclosed version of the shape UA-2c – body UA-2 [3]. The examples of similar 2D airfoils are calculated (see e.g., [3]). These facts open wide prospects for the use of unseparated shapes in order to improve the effectiveness of vehicles. Here we will analyze the drag and the lift characteristics of such shapes.

For slender unseparated hydrofoil (with a small thickness) we can use formula (11) and the estimation $S_{\mathrm{wet}} \approx 2Hb$ for its wetted area. Putting also $\varepsilon \approx 1$, the following estimation for the maximum value of the aerodynamic efficiency can be obtained:

$$k_{\max} \approx 0.5\sqrt{\frac{\pi\lambda_W}{2C_f}}. \qquad (16)$$

Using in (16) formulas (4) and (6), the following equations can be obtained in the case of laminar and turbulent flow respectively:

$$k_{\max,\text{lam}} \approx 0.54\lambda_W^{1/2}\,\text{Re}_H^{1/4},$$
$$k_{\max,\text{tur}} \approx 3.58\lambda_W^{1/2}\,\text{Re}_H^{1/14} \qquad (17)$$

where Re_H is the Reynolds number based on the chord length.

The drag on the unseparated wings at the optimal angle of attack corresponding to the maximum efficiency can be estimated as follows: $X = C_f S_{\text{wet}}\rho U^2$, since the pressure drag can be neglected and the induced drag is equal to the friction one. Then the optimal value of the lift force $Y_{\text{opt}} = k_{\max}X$, corresponding to the maximum efficiency, can be estimated with the use of (4), (6) and (17) for the laminar and the turbulent flow respectively:

$$Y_{\text{opt,lam}} \approx 1.43\lambda_W^{3/2}\,\text{Re}_H^{7/4}\,\rho\nu^2,$$
$$Y_{\text{opt,tur}} \approx 0.22\lambda_W^{3/2}\,\text{Re}_H^{27/14}\,\rho\nu^2. \qquad (18)$$

To estimate the optimal angle of attack α_{opt}, we can use the known linear dependence for the lift coefficient $C_y \equiv 2Y/(\rho U^2\lambda_W H^2) = 2\pi\alpha$ for a slender symmetric airfoil (see, e.g., [8]) and (18):

$$\alpha_{\text{opt,lam}} \approx 0.46\lambda_W^{1/2}\,\text{Re}_H^{-1/4},$$
$$\alpha_{\text{opt,tur}} \approx 0.07\lambda_W^{1/2}\,\text{Re}_H^{-1/14}. \qquad (19)$$

If the hull shape is close to the unseparated body of revolution, its lift force can be neglected at small angles of attack. The drag of such body can be estimated by (3) and (5) with removed last terms in each equation representing the pressure drag caused by separation. In the laminar case, formula (13) is preferable, since it takes into account the peculiarities of the axisymmetric flow, while the friction drag is estimated with the use of flat plate concept in Hoerner formulas (3)−(6).

Critical values of the Reynolds number, length and volume of the laminar shapes. Unseparated shapes reduce the pressure drag. If they also ensure laminar flow in the boundary layer, the friction drag can be also further reduced. Thus, the laminar unseparated vehicles must be the most effective in comparison with the turbulent ones, but they have to operate at small enough Reynolds numbers. In this section, we will estimate the critical values of Reynolds numbers, critical vehicle dimensions and velocities. In water it is possible to use supercavitating flow pattern (shown in Fig. 1, *b*, *c*). Its effectiveness we will discuss in next sections.

The laminar to turbulent flow transition in the boundary layer influences the skin-friction drag and depends on many parameters such as pressure gradient, surface roughness, pulsations in the ambient flow and so on (e.g., [8]). Nevertheless, according to the Tollmin−Schlichting−Lin theory (e.g., [21]) the boundary-layer on a flat plate remains laminar for any frequencies of disturbances, if

$$\text{Re}_\delta^* = \frac{\overline{U}\overline{\delta}^*}{\nu} < 420.$$

This inequality, taking into account the Blasius expression for displacement thickness (e.g., [8]) $\overline{\delta}^* = 1.721(\overline{x})^{1/2}\,\text{Re}_H^{-1/2}$ ($\overline{x}$ is the dimensionless coordinate based on the chord length), can be rewritten as follows: $\sqrt{\overline{x}\,\text{Re}_H} < 244.044$. If the boundary layer remains laminar over the entire surface of a slender unseparated airfoil, the critical value of the Reynolds number can be obtained by putting $\overline{x} = 1$:

$$\text{Re}_H^* = 59558. \qquad (20)$$

At smaller values of the Reynolds number the flow will be laminar at any slender unseparated wing.

Similar estimation has been done in [22] for the slender unseparated body of revolution with the use of the Mangler−Stepanov transformations:

$$\text{Re}_L\int_0^x R^2(\xi)d\xi < 59558 \qquad (21)$$

where $R(\xi)$ is the dimensionless radius of the body based on its length and the integral is proportional to the volume on the nose part of the body with the laminar boundary layer on its surface

$$V_{\text{lam}} = \pi L^3\int_0^x R^2(\xi)d\xi. \qquad (22)$$

If the boundary layer remains laminar over the entire surface ($V = V_{\text{lam}}$), formulae (21), (22) yield the critical value of the Reynolds number (see also [4]):

$$\text{Re}_L^* = \frac{59558\pi L^3}{V}. \qquad (23)$$

The maximum value of the laminar unseparated wing effectiveness corresponds to the critical value (20) and is equal to

$$k_{max,lam}^* \approx 8.44\lambda_W^{1/2} \qquad (24)$$

(it follows from (17)). The maximum chord length of the laminar wing can be determined from (20)

$$H^* = \frac{59558\nu}{U}, \qquad (25)$$

and its maximal lift force at the optimal angle of attack corresponding the maximum aerodynamic efficiency follows from (18) and (20):

$$Y_{opt,lam}^* \approx 3.25 \cdot 10^8 \rho\nu^2\lambda_W^{3/2}. \qquad (26)$$

Eq. (26) shows that the maximal lift force of the slender unseparated laminar wing is independent from the velocity and rapidly increases with the viscousity and the wing aspect ratio.

To estimate the maximal dimensions of the laminar body of revolution the information about its shape is necessary. For the unsepareted shape UA-2c (shown in Fig. 1a) and similar bodies with different thickness ratio D/L the simple formula can be used:

$$\frac{V}{L^3} = \gamma\left(\frac{D}{L}\right)^2 \qquad (27)$$

where dimensionless coefficient γ varies from 0.233 to 0.33 for D/L from 0.02 to 0.278 (body UA-2c). With the use of (23), (27) the maximum length and volume of the laminar unseparated body of revolution can be determined:

$$L^* = \frac{1.87 \cdot 10^5\nu}{\gamma U}\left(\frac{L}{D}\right)^2,$$
$$V^* = \frac{6.54 \cdot 10^{15}\nu^3}{\gamma^2 U^3}\left(\frac{L}{D}\right)^4. \qquad (28)$$

With the use of Froude number (28) can be rewritten as follows:

$$L^* = \left[\frac{1.87 \cdot 10^5\nu}{\gamma Fr_L \sqrt{g}}\right]^{2/3}\left[\frac{L}{D}\right]^{4/3},$$
$$V^* = \frac{3.5 \cdot 10^{10}\nu^2}{\gamma g Fr_L^2}\left[\frac{L}{D}\right]^2. \qquad (29)$$

The calculations of the dimensions of the laminar unseparated vehicle are presented in Fig. 3 (water at $\nu = 1.3 \cdot 10^{-6}$ m²/s) and Fig. 4 (air at different attitudes).

Drag on slender body of revolution for attached and supercavitating flow patterns. The drag on a slender unseparated body of revolution is mainly determined by the friction in the boundary layer. If
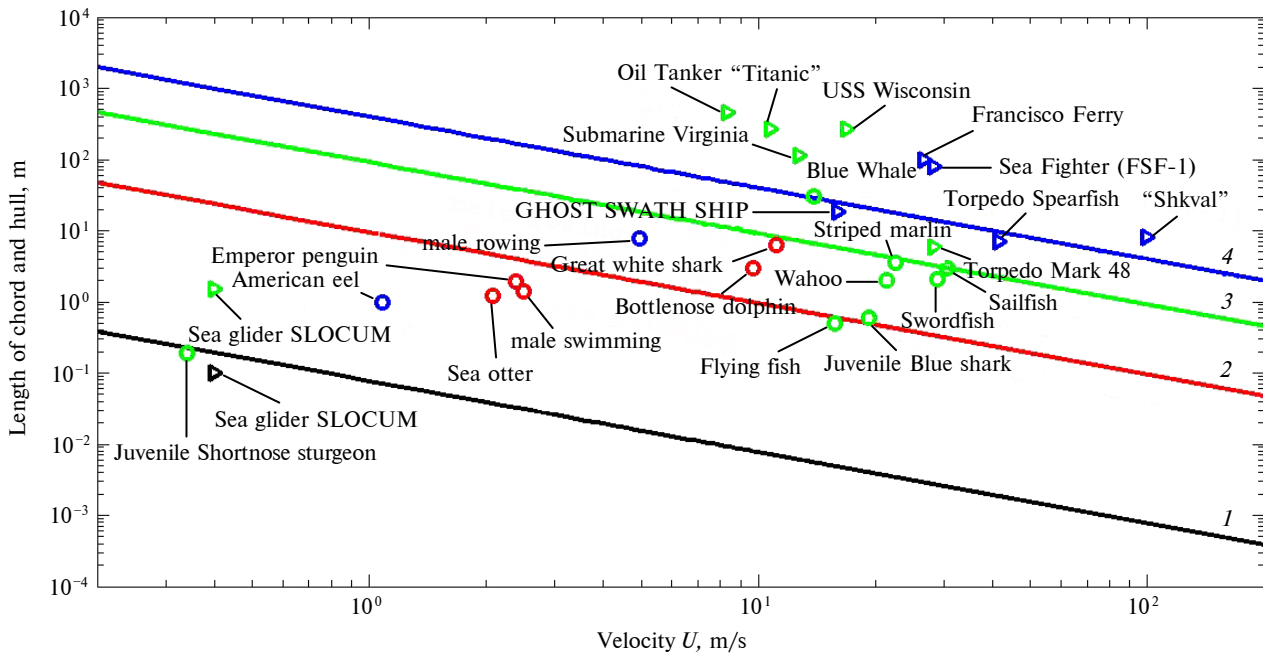

Fig. 3. The maximum chord length of the laminar unseparated wing (eq. (25)) in water (line *1*).The maximum length of the laminar unseparated body of revolution (eq. (28)) in water at different values of the thickness D/L = 0.278; 0.1; 0.05 (lines *2−4* respectively). "Circles" represent data for animals; "triangles" − for vehicles
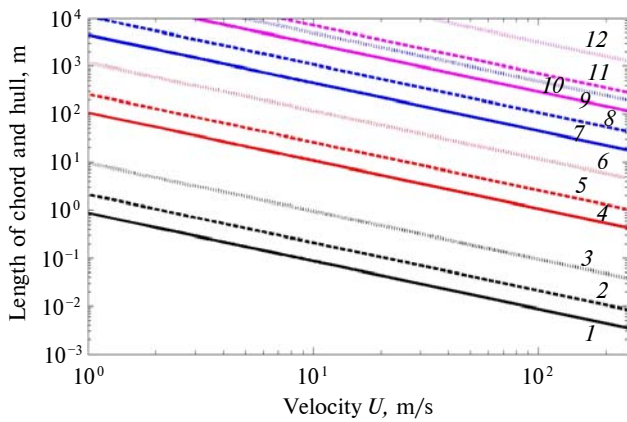
Fig. 4. The maximum chord length of the laminar unseparated wing (eq. (25)) in air (lines *1−3*). The maximum length of the laminar unseparated body of revolution (eq. (28)) in air at different values of the thickness D/L = 0.278 (lines *4−6*); 0.05 (lines *7−9*) and 0.02 (lines *10−12*). The values were calculated at 0 km (solid lines *1, 4, 7, 10*); 10 km (dashed lines *2, 5, 8, 11*) and 20 km (dotted lines *3, 6, 9, 12*) height above sea level

its volume does not exceed V_{lam}, the volumetric drag coefficient C_V is given by formula (13). Otherwise, the laminar-to-turbulent transition must be taken into account. Simple estimations of the drag can be obtained with the use of Mangler−Stepanov transformations and the Blasius flat-plate skin-friction in the laminar part of the boundary layer (see details in [22]) and formula (6) in its transitional and turbulent part. The results are show in Fig. 5 by solid lines for different values of the body thickness
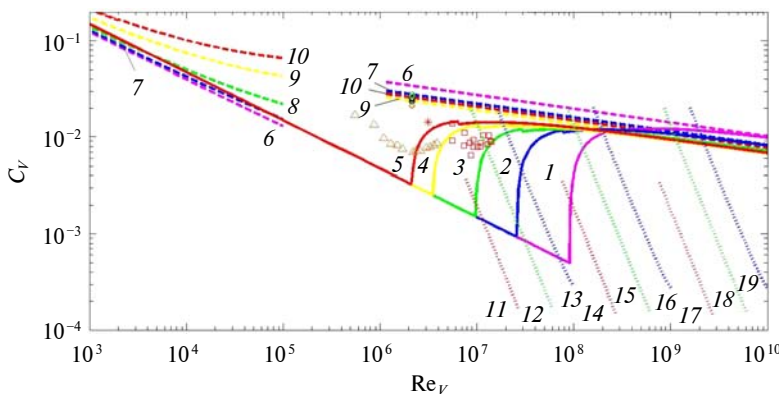

Fig. 5. Volumetric drag coefficients for axisymmetric hulls. Unseparated shapes are represented by solid lines *1−5*; conventional shapes (Hoerner formulae (3)−(6)) — by dashed lines *6−10*. The body thickness D/L = 0.02 (lines *1* and *6*); 0.05 (lines *2* and *7*); 0.1 (lines *3* and *8*); 0.2 (lines *4* and *9*); 0.278 (lines *5* and *10*). Markers present the experimental data. Dotted lines *11−19* show the volumetric drag coefficients of the super-cavitating slender axisymmetric hulls for different volume: 0.001 m³ (lines *11−13*); 1 m³ (lines *14−16*); 1000 m³ (lines *17−19*) and the depth of movement: 2 m (lines *11, 14, 17*); 50 m (lines *12, 15, 18*); 200 m (lines *13, 16, 19*)

D/L. The minimum points correspond to the critical values of the Reynolds number (23). For comparison the drag coefficients of conventional shapes (eqs. (3)−(6)) are presented by dashed lines. The experimental data are shown by markers for different bodies of revolution.

It can be seen that on very slender bodies of revolution ($D/L < 0.05$) C_V could be smaller than 0.001 at the Reynolds numbers close to the critical one. At greater Re_V the volumetric drag coefficient rapidly increases and approaches value

$$C_V \approx 0.01 \qquad (30)$$

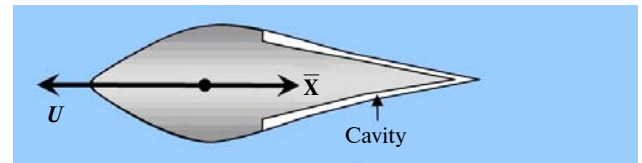which is practically independent from the thickness ratio.

Fig. 6. Unseparated body of revolution (non-standard cavitator) and cavity, which needs no closing body

The tail part of an underwater unseparated hull can be covered by the cavity, which closes itself (without any closing rigid body or re-entrant jet, see Fig. 6). Then the hull's pressure drag is still near to zero (due to D'Alambert paradox). The skin-friction drag on such vehicle can be reduced, since the large part of its surface has no contact with the water. In particular, the volumetric drag coefficient can be estimated as follows for the laminar boundary-layer [23]:

$$C_V = \frac{4.7}{\sqrt{\text{Re}_V}} \sqrt{\frac{V_b}{V}} \qquad (31)$$

where V_b is the volume of the body's part wetted by water.

In order to realize the flow pattern shown in Fig. 6, a special investigation has been done in [24]. It was shown that the drag diminishing of 31 % (in comparison with the unseparated flow pattern $V_b = V$) is possible. Formula (31) yields the estimation $C_V \approx 5 \cdot 10^{-4}$ for the slender body with D/L = 0.046 [11, 24]. This value is 14 times less than the volumetric drag of the underwater apparatus "Dolphin" measured

at $\mathrm{Re}_V = 8.5 \cdot 10^6$ (see [25], "square" markers in Fig. 5).

For the underwater supercavitating hulls shown in Fig. 1, *b*, *c*, the friction drag on a small cavitator can be neglected, but its pressure drag yields the main part of the total drag. The analytical formulas presented in [6] allow calculating the volumetric drag coefficient for the case of slender conical cavitator (see Fig. 1, *c*). The results are shown in Fig. 5 by dotted lines at different values of the hull volume (which is close to the cavity one, such as shown in Fig. 1, *b*) and the depth of motion *h*. It can be seen that supercavitation allows diminishing the volumetric drag coefficients up to values $C_V \approx 2 \cdot 10^{-4}$. Further drag diminishing is limited by very large values of the cavity (hull) aspect ratio at higher velocities (see Fig. 2). All data presented in Fig. 5 are limited by $D/L > 0.02$.

Commercial efficiency estimations. Formulas (9), (13) and (30) allow estimating the vehicle drag-to-weight ratio in the cases of the laminar unseparated and the turbulent hulls respectively:

$$\frac{1}{k_{\mathrm{lam}}} = \frac{1-\alpha}{k_W} + 2.35\alpha\sqrt{\frac{\nu U^3}{g^2 V}}$$

$$= \frac{1-\alpha}{k_W} + 2.35\sqrt{\frac{\rho\alpha\nu U^3}{g^2 m}}, \qquad (32)$$

$$\frac{1}{k_{\mathrm{tur}}} \approx \frac{1-\alpha}{k_W} + 0.005\alpha\mathrm{Fr}_V^2 = \frac{1-\alpha}{k_W} + \frac{U^2}{200g}\sqrt[3]{\frac{\alpha^2\rho}{m}}. \quad (33)$$

For the supercavitating vehicle with a slender conical cavitator (see Fig. 1, *c*) formulae (2), (8), and (9) yield:

$$\frac{1}{k_{SC}} = \frac{1}{k_W} + 0.5\alpha C_V \mathrm{Fr}_V^2 = \frac{1}{k_W}$$

$$+ \alpha C_{Vh} \frac{(h+10)}{V^{1/3}} \approx \frac{1}{k_W} + 0.1\alpha \frac{(h+10)}{V^{1/3}} \qquad (34)$$

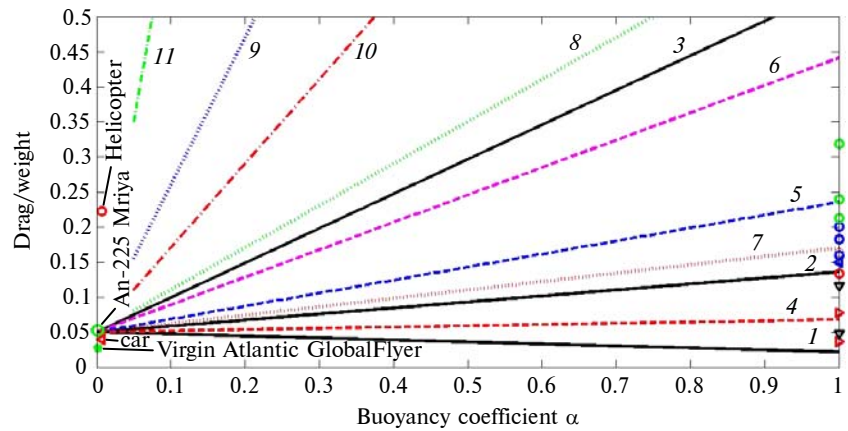Linear dependences (32)–(34) versus buoyancy coefficient are shown in Fig. 7.

Fig. 7. Drag-to-weight ratio for unseparated and supercavitating vehicles for $k_w = 20$. Solid lines *1–3* correspond to the laminar unseparated hull with $V = V_{\mathrm{lam}}$ (formula (36) at $\mathrm{Fr}_L = 2$, 5, and 10 respectively). Dashed lines *4–6* represent turbulent unseparated hull (eq. (33), $\mathrm{Fr}_L = 2$ and $D/L = 0.278$, 0.05, and 0.02 respectively). Dotted lines *7–9* correspond to the supercavitating vehicle (eq. (34), $V = 1000$ m^3, $h = 2$ m, 50 m, and 200 m respectively). Dashed-dotted lines *10* and *11* correspond to the supercavitating vehicle (eq. (34), $V = 1$ m^3, $h = 2$ m, and 50 m respectively). Markers show the experimental points

If the velocity and the volume of the unseparated hull are fixed, the minimum value of the drag-to-weight ratio is achieved at $\alpha \to 0$, or when $\alpha = 1$, depending on the value of the coefficient k_W. The critical values k_W^* correspond to the horizontal straight lines (32), (33) and are equal to:

$$k_{W,\,\mathrm{lam}}^* = 0.43\sqrt{\frac{g^2 V}{\nu U^3}} = 0.43\sqrt{\frac{\alpha m g^2}{\rho\nu U^3}},$$

$$k_{W,\,\mathrm{tur}}^* \approx 200\mathrm{Fr}_V^{-2} = \frac{200 g \alpha^{1/3} m^{1/3}}{U^2 \rho^{1/3}}$$

for the laminar and the turbulent case respectively. If $k_W < k_W^*$ the maximum of the commercial efficiency (the minimal value of $1/k$) is achieved at $\alpha = 1$ (i.e., the most effective vehicles are neutral buoyant ones — ships, airships, submarines), otherwise the buoyancy parameter must be as small as possible. Formula (34) and Fig. 7 show that optimal supercavitating vehicles must have minimal possible value of α (in particular, to be heavy than water).

If the velocity and mass of the vehicle are fixed, the nonlinear dependences (32), (33) have maxima at some values of α and minimum value of the drag-to-weight ratio is achieved at $\alpha \to 0$, or when $\alpha = 1$, depending on the value of the coeffi-

cient k_W. Its critical values k_W^{**} can be calculated from (32), (33):

$$k_{W,\text{lam}}^{**} = 0.43g\frac{\sqrt{m}}{\sqrt{\rho\nu U^3}} = 0.43g\frac{\sqrt{V}}{\sqrt{\alpha\nu U^3}},$$

$$k_{W,\text{tur}}^{**} \approx \frac{200gm^{1/3}}{U^2\rho^{1/3}} = \frac{200gV^{1/3}}{\alpha^{1/3}U^2}$$

(35)

for the laminar and the turbulent case respectively. If $k_W < k_W^{**}$ the maximum of the commercial efficiency (minimal value of $1/k$) is achieved at $\alpha = 1$, otherwise the buoyancy parameter must be as small as possible.

Efficiency of a laminar unseparated vehicle will be maximum at maximal possible volume of the hull $V = V_{\text{lam}}$ (see (32)) and maximum possible length of the wind chord (see (25)). Then formulae (22), (24), and (32) yield:

$$1/k = (1-\alpha)/k_W + 0.00543\alpha Fr_L^2,$$

$$k_{W,\text{lam}}^* = 184Fr_L^{-2},$$

(36)

$$Fr_{L,\text{lam}}^* = 13.6k_W^{-1/2} = 4.67\lambda^{-1/4}.$$

If the Froude number is smaller than $Fr_{L,\text{lam}}^*$, the neutral buoyant vehicles are preferable.

For the supercavitating vehicle, (34) yields the estimation of the critical number $k_{W,SC}^{**}$ $= 10V^{1/3}[\alpha(h+10)]^{-1} < \alpha^{-1}V^{1/3}$. At greater values of k_W the pressure drag on a cavitator (see Fig. 1) is higher than the drag connected with weight supporting (i.e., the drag of the wing piercing the cavity or the planning drag on the hull). For small vehicles the values of $k_{W,SC}^{**}$ are rather small. It means that the drag on the cavitator is prevailing.

Efficiency estimations for running. To estimate the efficiency of running, we need the value of k_W or the average drag coefficient $1/k_W$, corresponding to the weight support. We shall modify the approach proposed in [26], which assumes running as series of jumps and the energy of the vertical motion as wasted to support the horizontal motion. Then this wasted kinetic energy equals $0.5mv^2$ (v is the vertical velocity in the beginning of the jump). By dividing this energy by the duration of the jump $2v/g$ (air drag is neglected) the wasted capacity $0.25mgv$

and the average drag coefficient $1/k_W = 0.25v/U$ were estimated in [26]. With the use of an unrealistic assumption $v = U$ (it means that jump height must be approximately 5 m for an athlete with the 10 m/s running velocity) the value $1/k_W = 0.25$ was proposed in [26].

Let us calculate the vertical velocity with the use of the duration the jump and its length $l_j = 2Uv/g$. Then the average drag coefficient can be estimated as follows:

$$1/k_W = 0.25v/U = 0.125l_jg/U^2.$$

(37)

For example, Usain Bolt makes 41 jumps during his word record 100 m running ($U = 10.44$ m/s). Formula (37) yields the value $1/k_W \approx 0.027$, which is almost 10 times smaller than estimation [26]. In the case of the fastest running animal − cheetah − (acinonyx jubatus, $U = 31$ m/s, $l_j \approx 7$ m), $1/k_W \approx 0.0089$. For a hare (genus lepus, $U = 18$ m/s, $l_j \approx 3$ m), $1/k_W \approx 0.011$. We use the data about animal mass, length and velocity from [27] and other information available in internet.

To check the assumption that the air drag can be neglected for running, let us use (32) and (33) and calculate the critical values of k_W, when the aerodynamic drag is equal to the one connected with the weight supporting:

$$k_{W,\text{lam}}^{***} = 0.43\frac{g(1-\alpha)\sqrt{m}}{\sqrt{\alpha\rho\nu U^3}} = 0.43\frac{g(1-\alpha)\sqrt{V}}{\alpha\sqrt{\nu U^3}},$$

$$k_{W,\text{tur}}^{***} \approx \frac{200g(1-\alpha)m^{1/3}}{U^2\alpha^{2/3}\rho^{1/3}} = \frac{200g(1-\alpha)V^{1/3}}{U^2\alpha}.$$

(38)

Using in (38) the values $\rho \approx 1.225$ kg/m^3, $\nu \approx 1.46\cdot10^{-5}$ m^2/s, $\alpha \approx 1.225\cdot10^{-3}$, the following estimations can be obtained: in the case of human record 100 m running ($m = 94$ kg), $k_{W,\text{lam}}^{***} \approx 8173$, $k_{W,\text{tur}}^{***} \approx 6666$; for a cheetah ($m = 65$ kg) and for a hare ($m = 2$ kg) $k_{W,\text{lam}}^{***} \approx 1328$ and $k_{W,\text{lam}}^{***} \approx 527$ respectively. So large values of $k_{W,\text{lam}}^{***}$ show that the air drag can be neglected by running. May be, it could be some exceptions only for very small animals, like German cockroach (blattella germanica, $m = 20$ mg, $U = 1.3$ m/s, $k_{W,\text{lam}}^{***} \approx 86$).

Since the air drag is negligible, the cost of running $1/k \approx 1/k_W$ and is independent from

speed. Such conclusion is in agreement with the previous investigations (see e.g., [26]). The real metabolic cost of human running is approximately 4 $Jkg^{-1}m^{-1}$ (see, e.g., [16]) or 0.41. This value is 15 times greater than the obtained above estimation 0.027. It means that only a small part of the energy released in human body is transformed into the energy of movement, i.e., the propulsion efficiency coefficient η is rather small.

Results and discussion

Comparison of the drag coefficients for conventional, unseparated and supercavitating hulls. Evidently, the hull drag is important for the neutral buoyant vehicles (such as conventional ships, SWATH ships, airships, submarines) or quasi neutral buoyant ($\alpha \to 1$, such as underwater gliders, conventional torpedoes), since it is the main part of the total drag. Fig. 5 shows that there is a rather large range of the Reynolds number $10^6 \le \mathrm{Re}_V \le 10^8$, where the use of unseparated shapes yields very substantial reduction of the drag in comparison with the conventional bodies of revolution.

In water at $\mathrm{Re}_V > 10^7$ the supercavitating flow pattern can be preferable. Both for the unseparated and for supercavitating vehicles, the thickness ratio D/L must be as small as possible to achieve smaller values of the drag coefficient. Figs. 3 and 4 demonstrate that the laminar unseparated hulls of rather large dimensions can be used at large range of the velocities in water and in air. The length and volume of such hulls increase with diminishing of D/L and increasing the height above sea level. These facts creates challenges to strengthen the construction of the hulls in order to decrease D/L, to withstand heavy longitudinal forces and to avoid buckling.

In order to estimate the importance of the unseparated hulls in the design of non-neutral buoyant vehicles, estimations (38) can be used to compare the drag of hulls and one connected with the weight support. For example, for a typical car ($m = 1$ t, $V = 10$ m^3, $U = 40$ m/s, $\rho \approx 1.225$ kg/m^3, $\nu \approx 1.46 \cdot 10^{-5}$ m^2/s) $\alpha \approx 0.012$, $\alpha \approx 0.012$, and the critical values $k_{W,\mathrm{lam}}^{***} \approx 1112$, $k_{W,\mathrm{tur}}^{***} \approx 221$ are greater than $k_W \approx 100$. It means that the drag on an unseparated hull is smaller than the friction drag on wheels. Similar situation takes place for buses,

tracks and trains, where the critical values are expected to be higher due to the greater mass.

Let us estimate the aerodynamic drag and dimensions of the slender unseparated shape (similar to shown in Fig. 1, *a*) at the $\mathrm{Re}_V \approx 5.9 \cdot 10^6$ (the value, corresponding to the mentioned above typical car). At this Reynolds number the ideal shape can be laminar and its drag can be estimated with the use of (13) as follows: $C_V \approx 0.0019$. Formula (2) allows recalculating the drag coefficient with the use of the frontal area $A = \pi D^2/4$. To find the diameter of the corresponding ideal laminar hull let us use the condition $V = V_{\mathrm{lam}} = 10$ m^3 and formulas (27), (28), $\gamma \approx 0.3$. Then $D/L \approx 0.137$, $L \approx 12.1$ m, $D \approx 1.66$ m and the frontal drag coefficient $C_{xA} \approx 0.0041$ for this ideal laminar unseparated body of revolution. For the turbulent flow pattern estimation (30) yields $C_{xA} \approx 0.021$. These values are much smaller than the drag measurements on the best-shaped commercial cars (12−60 times), [28], and 2.5−13 times smaller than the frontal drag coefficient of the special car Eco-runner ($C_{xA} \approx 0.0512$), [28, 29].

Presented estimations show that the laminar unseparated shapes can be used for special cars (e.g., [29, 30]) in order to reduce their drag. To make the conventional cars compact, comfortable for passengers and stable on curved roads, the car designers use typical box-like shapes and try to reduce the negative effects of separation (which is inevitable on such hulls). The payment for these advantages can be very high and can cause drastic increase of the aerodynamic drag (which can significantly exceed the drag on wheels).

For example, the Formula one car has unexpected high aerodynamic (and total) drag $C_{xA} = 0.7−1.1$ (see, e.g., [28]). There is the payment for stability on curved loops, which needs a large downforce. Its value is greater than about two weight of the car (702 kg [31]). To create this force the wings and special hull shape are used. The efficiency of wings is very limited, since it is impossible to use the laminar flow pattern and to increase λ_W. Indeed, at the velocity of 100 m/s the maximum chord length of a laminar wing is approximately 8.7 mm (see (25), Fig. 4). Since the width of the car is limited by 180 cm, the maximum aspect ratio of the laminar wind is 207. Then the maximum downforce at an optimal angle of attack $Y_{\mathrm{opt,lam}}^* \approx 253N$ (see (26)) and is not enough for stability. To have

the downforce of 7000 N at one wing, we need extending the chord at least 27.6 times, to have $\lambda_W < 7.5$ and the ratio of the car weight to the drag on two wings must be less than 12 (see (24)). Thus, the drag connected with the creating downforce is the overwhelming part of the total drag on the Formula one car.

Fig. 4 and formula (28) show that the laminar unseparated shapes can be used also for large subsonic airplanes provided their D/L ratio is small enough. For example, at the velocity 250 m/s, the height above see level 10 km ($\nu \approx 3.53 \cdot 10^{-5}$ m^2/s) and $L/D = 20-50$, the maximum length of such hulls varies from 43 m to 284 m and the maximum volume of the laminar hull varies from 49 m^3 to 2123 m^3. The last value approaches to the hull volume of the largest airplane Antonov An-225 "Mriya", [32]. Using (38) yield $k_{W,\text{lam}}^{***} \approx 587$ and $k_{W,\text{tur}}^{***} \approx 54.8$ at $V = 43$ m^3, $\alpha \approx 0.002$. It means that the drag of this laminar hull (and greater ones) can be neglected in comparison with the drag on the wing, since its aerodynamic efficiency is typically smaller than 60, [33] (the same value follows from (24) at $\lambda_W \approx 50$).

The huge difference between $k_{W,\text{lam}}^{***}$ and $k_{W,\text{tur}}^{***}$ shows that the use of the laminar unseparated hulls can give a significant decrease of their drag. Nevertheless, in order to have compact and comfortable airplanes, the conventional shapes can be preferable. For example, the hull of Solar Impulse 2 plane, [34], which rounded globe with the use of solar energy only, looks not very good streamlined. For its velocity 17 m/s, 2300 kg of mass, the attitude of 8300 m ($\rho \approx 0.51$ kg/m^3, $\nu \approx 3.02 \cdot 10^{-5}$ m^2/s) and $\alpha \approx 0.01$, equation (24) yields $k_{W,\text{tur}}^{***} \approx 2406$ and the conclusion that the hull drag can be neglected. Estimation (35) yields very high values of $k_{W,\text{lam}}^{**} \approx 739$ for Solar Impulse 2. It means that for a vehicle with the same mass, velocity and attitude is much better to use the neutral buoyant option. The commercial efficiency of a corresponding airship would be $k \approx 727$. Its characteristics can be estimated as follows: $V = m/\rho \approx 4510$ m^3, $L/D = 9.7$, $\gamma \approx 0.27$, $L = 116$ m. The upper surface of the envelope (half of the total wetted area and suitable for fixing solar cells) is greater than 1000 m^2 and is 5 times larger than the wing area of Solar Impulse 2.

Unseparated wings and vehicles. Vehicles or animals, which ensure a laminar attached flow pattern are expected to be the most effective, since separation and turbulence cause intensive vortexes in the flow, increase of drag and noise. Fig. 5, formulae (4) and (25) show that minimal drag coefficients and the maximum commercial efficiency (see (36)) correspond to the maximum possible volume of the hull $V = V_\text{lam}$ and maximum possible length of the wind chord.

The applications of the laminar wings are limited due to the small values of the maximum chord length and corresponding maximal lift force at optimal angle of attack (see Figs 3, 4 and formulas (25), (26)). Even at $\lambda_W = 50$, the maximum lift force equals 194 N for water ($\nu \approx 1.3 \cdot 10^{-6}$ m^2/s) and $Y_{\text{opt,lam}}^* \approx 30$; 59.2 and 261 N for the steady movement in air at the attitudes 0, 10 and 20 km respectively. For smaller values of the wing aspect ratio, corresponding values are smaller, e.g. $Y_{\text{opt,lam}}^* \approx 2.7$ N and 7.6 N for $\lambda_W = 10$ and 20 respectively (for air at zero attitude).

It means that we can expect to observe the laminar flow only on wings of small vehicles or small birds. E.g., the weight the fastest bird swift ($m \approx 40$ g) – can be supported by the laminar wing. Another example is the sea glider, on which only the small percent of weight is supported by the wing, [35]. But the hybrid airship Airlander-10 is too heavy and 40 % of its weight cannot be supported by the laminar wing [36].

Decreasing the chord length slowly decreases the wing efficiency (which is proportional to $\text{Re}_H^{1/4}$, see (17)) and rapidly diminishes the lift force (which is proportional to $\text{Re}_H^{7/4}$, see (18)). For example, for the bee ($\lambda_W \approx 7$, $U \approx 17$ m/s, $H \approx 2.3$ mm, $m \approx 100$ mg, $\text{Re}_H \approx 2680$, $\alpha \approx 0.0016$) $k_{\text{max,lam}} \approx 10.3$; $Y_{\text{opt,lam}} \approx 0.0069$ N and $k_{W,\text{lam}}^{***} \approx 3.6$ (according to (17); (18) and (38) respectively). These estimations show that the laminar wing could provide the lift sufficient to support the bee weight, but the drag on its body is greater than the drag on the optimal wing, and the weight-to-drag ratio is only 2.6 (according to (32)). May be it is the reason why insects use very specific unsteady flow pattern with the very high frequency wing oscillations [37] (for which the presented steady flow estimations are not valid).

Another conclusion can be drawn up: the mini-aturization of the vehicles can lead to increasing their drag coefficients and cause decreasing their commercial efficiency. Since the power-to-weight ratio or the capacity-efficiency increases with decreasing of commercial efficiency (see previous section), the maneuverability of small vehicles can be very high. E.g., the capacity-efficiency of the bee $C_E = U/k_W \approx 17/2.6 \approx 6.5$ m/s is 23 times greater than one of cheetah $C_E \approx 31 \cdot 0.0089 \approx 0.28$ m/s (the estimations from the previous section were used). In the next section we shall speak about the capacity-efficiency in details.

If the Reynolds numbers are higher than estimation (20), the turbulent unseparated wings must be used. If such a wing ensures the attached flow pattern at the optimal angle of attack (see (19)) and the Reynolds number is much higher than (20), the turbulent flow pattern yields better wing efficiency than in the laminar case (see (17)).

Let us calculate the efficiency of the albatross ($\lambda_W \approx 12$, $U \approx 35$ m/s, the wing span $b \approx 3.4$ m, $m \approx 10$ kg, $\mathrm{Re}_H \approx 679000$, $\alpha \approx 0.0015$ [38]) $k_{\mathrm{max,tur}} \approx 32.4$; $Y_{\mathrm{opt,tur}} \approx 422\,N$.

It can be seen that optimal cruising speed of the albatross could be approximately twice smaller in order to support its weight. Fig. 4 show that its body length is small enough to ensure laminar flow pattern. Then formula (32) yields the values of total weight-to-drag ratio between 30 and 31 (for different values of the velocity). The observations of the albatross flight show the values between 22 and 23 [39]. In the case of airplanes the discrepancies between theoretical estimations and experimental value of commercial efficiency are more substantial. E.g., for Antonov An-225 "Mriya" ($\lambda_W \approx 8.7$, $U \approx 220$ m/s, $H \approx 10.2$ m, $\mathrm{Re}_H \approx 6.4 \cdot 10^7$ (at the attitude 10 km) [32]) $k_{\mathrm{max,tur}} \approx 38$ (see (17)). Since the drag on the hull can be neglected (in comparison with the drag on the wing, see previous section), the theoretical weight-to-drag ratio is close to 38 and is twice greater than the experimental value $k \approx 19$. It means that the efficiency could be improved with the use of unseparated shapes.

Presented estimations allow explaining the flight of pterosaurs. The dimensions of these fossil animals (the wind span reaches 11 m) seem to be too big for flight, [40]. Since the maximal wing span of the pterosaur is approximately 3 times larger than in the case of albatross, we can expect its weight is 27 times greater, i.e. $m \approx 270$ kg. Let us suppose that the speed of pterosaur and its wing aspect ratio coincide with ones for albatross ($U \approx 35$ m/s, $\lambda_W \approx 12$), the $\mathrm{Re}_H \approx 2 \cdot 10^6$, $k_{\mathrm{max,tur}} \approx 35$; $Y_{\mathrm{opt,tur}} \approx 3500\,N$. Therefore the weight of the pterosaur could be supported even at smaller velocity $U \approx 30$ m/s. The capacity-efficiency of pterosaur can be estimated as follows: $C_E = U/k_W \approx 35/35 = 1$ (provided its body shape was laminar and unseparated, and the drag on the body can be neglected in comparison with the drag on the wings). This value is even smaller than for albatross, i.e. the pterosaur did not need any special metabolic power to be airborne.

During takeoff the velocity is much smaller than in the cruising flight and it is difficult to support the weight. The problem is solved by increasing the angle of attack and by changing direction of the thrust on flapping wing of airborne animals. Since the stall angle (at which the lift force attains its maximum and cannot be increased due to separation) is limited, the optimal angle of attack must be as small as possible to ensure takeoff at low velocities (in comparison with the cruising one). With the use of (19) the optimal angles of attack can be estimated as 4.9 and 5.3 degrees for the pterosaur and albatross respectively. It means that their takeoff characteristics are similar, provided both animals have nice shaped wings with large enough stall angles.

A high takeoff velocity could be an additional limitation for the wing aspect ratio. The commercial efficiency increases with increasing of λ_W (see (17), (32), (33)). On the other hand, the optimal angle of attack also increases. E.g., for Antonov An-225 "Mriya" $\alpha_{\mathrm{opt,tur}} \approx 3.3°$. At $\lambda_W = 50$ a vehicle with the same value of Reynolds number would have $\alpha_{\mathrm{opt,tur}} \approx 7.9°$. This fact once again shows the importance of using unseparated airfoil profiles in order to increase the stall angle of attack.

Capacity-efficiency of vehicles and animals. Let us estimate first the capacity-efficiency of neutral buoyant vehicles and aquatic animals (their buoyancy coefficient α is close to 1.0) with the use of formula (15) and the Froude number Fr_L. The values are shown in Fig. 8 by circles (small markers correspond to vehicles, middle markers — animals, big markers — male champions sport activity). It can be seen regular increase of the capacity-efficiency versus the Froude number. The experimental values are in good agreement with the theoretical estimation $C_E = U/k \approx 0.00543U\mathrm{Fr}_L^2$, which follows from (36) and is shown by lines for different values of hull/body
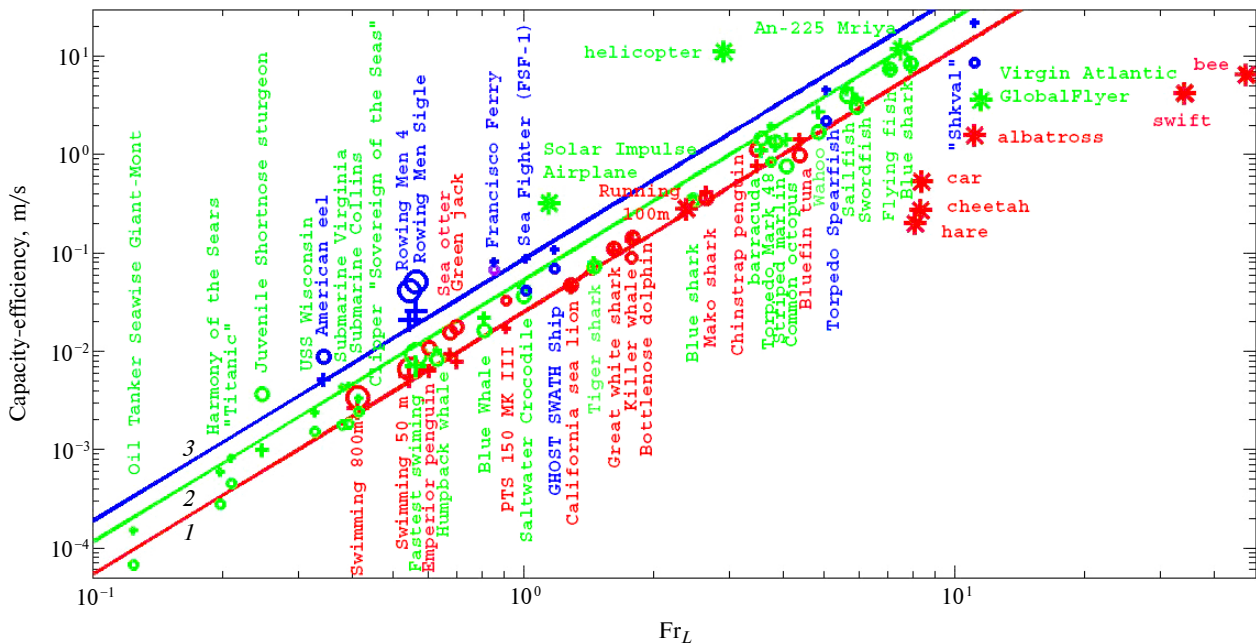
Fig. 8. Capacity-efficiency (m/s) versus Froude number Fr_L for aquatic ("crosses" and "circles"), terrestrial and airborne ("stars") animals and vehicles. Theoretical estimations based on (36) are presented by lines *1−3* for D/L = 0.278, 0.1, and 0.05 respectively

thickness ratio D/L and $\nu \approx 1.3 \cdot 10^{-6}$ m^2/s. Since eq. (36) corresponds to the minimum of the volumetric drag coefficient on the slender unseparated body of revolution ($V = V_{\text{lam}}$) and the maximal value of the weight-to-drag ratio k, the shown lines correspond to the vehicles and animals with the maximum commercial efficiency. Since vehicles and animals have individual values of D/L and the temperature of water changes, the same characteristic was calculated for every object and presented in Fig. 8 by crosses.

It can be seen that in the case of animals the difference between real ("cirles") and theoretical ("crosses") values of C_E is much smaller than for vehicles, and the real values for animals are mostly higher than the theoretical ones (especially for small enough animals with the length smaller than estimation (28) or (29), e.g., juvenile shortnose sturgeon, american eel, male swimming and rowing). Thus, we can conclude that shapes of the aquatic animals can be close to the optimal laminar unseparated ones. E.g., the highest values of C_E correspond to juvenile blue shark (8.5 m/s) and flying fish (7.4 m/s) and the case $V < V_{\text{lam}}$. Larger animals ($V > V_{\text{lam}}$) have smaller values of capacity-efficiency and their theoretical characteristics exceed the

real ones (e.g. sailfish, swordfish, blue whale, great white shark).

The values of C_E for the best swimming animals can be much greater than for vehicles and approach $C_E \approx 8.5$ for the unseparated vehicle with the mass, velocity and volume equal to ones of the supercavitating torpedo Shkval ([41], the estimation $\alpha \approx 0.26$ was used in (14) and (26)). According to the formula (34) the capacity-efficiency of small enough supercavitating vehicles can be estimated as $C_E \approx 0.1\alpha U(h+10)V^{-1/3}$ and equals 44 m/s and 58 m/s for the torpedo Shkval moving at depth 5 and 10 m respectively. These high values of C_E are related to the low values of the commercial efficiency. According to (34) $1/k \approx 0.1\alpha(h+10)V^{-1/3}$, and yields 0.44 and 0.58 for the torpedo Shkval moving at depth 5 and 10 m respectively. Such as low commercial efficiency estimations can be obtained for common torpedoes Spearfish [42], and Mark 48 [43], with the values $1/k \approx 0.69$ ($\alpha \approx 0.93$) and $1/k \approx 0.32$ ($\alpha \approx 0.79$) respectively (formula (33) and $k_W = 10$ were used).

Formula (14) was used to estimate the capacity-efficiency of the male champions running and airborne animals and vehicles moving in air. The results

are presented in Fig. 8 by "stars". In comparison with the aquatic animals, the values of C_E are not so much dependent on the Froude number. E.g., the male run champion has the efficiency $C_E \approx U/k_W \approx 0.28$ m/s ($\mathrm{Fr}_L \approx 2.4$), the same value of efficiency can be obtained for cheetah ($\mathrm{Fr}_L \approx 8.4$), and 0.2 m/s fore hare (1) (see velocity and friction coefficient data in previous section).

The capacity-efficiency values for the human sport activity show that we are much effective runners than swimmers. E.g., for male freestyle swimming $C_E \approx 0.0067$ m/s and $C_E \approx 0.0034$ m/s on distances 50m and 800m (world records). Assuming the same metabolic rate during some fixed period of activity (this value diminishes with the increase of duration of activity), we can conclude that humans can covert their muscles energy in running velocity much better than in the case of swimming. It is expectable, since humans were developed by evolution as terrestrial animals. Better shaping can increase the capacity-efficiency. We can see this comparing the values for swimming and rowing $C_E \approx 0.051$ m/s (Lightweight Men Single, best time). It can be seen that the low drag elongated shape of the racing boat (and may be higher propulsion coefficient) allows up to 10 times increase the efficiency of movement.

It must be noted that real values of the power-to-weight ratio are much greater than the capacity-efficiency. For example, the maximum metabolic rate of human athletes is approximately 2.9 m/s (28 W/kg) [16] and is 10 times greater than the capacity-efficiency of 100 m running. Similar large differences occur in the case of submarines (see [4]) and for the Formula One car (its power-to-weight ratio is approximately 107 m/s). Such huge differentces can be explained by non-optimal shape and small value of the locomotion coefficient η.

Conclusions

Simple analytic formulae and computational results were obtained for the drag coefficients, drag-to-weight and power-to-weight ratios and were ap-

plied for different terrestrial, aquatic and airborne vehicles, animals and human sport activity. The critical Reynolds numbers of the laminar-to-turbulent transition on slender unseparated shapes and corresponding lengths of the wing chord and hull were calculated. Obtained theoretical results can be used in conceptual design of different vehicles. A reliable estimation of the running drag coefficient was obtained.

The obtained theoretical results show that there is a rather large range of the volumetric Reynolds number $10^6 \le \mathrm{Re}_V \le 10^8$, where the use of unseparated shapes yields very substantial reduction of the drag in comparison with the conventional bodies of revolution. For the high-speed underwater motion at $\mathrm{Re}_V > 10^7$, the supercavitating flow pattern can be preferable. This drag reduction opens up prospects for designing different kinds of effective airborne, terrestrial and high-speed underwater vehicles. Both for the unseparated and for supercavitating hulls, the diameter-to-length ratio must be as small as possible to achieve smaller values of the drag coefficient and to increase the commercial efficiency.

It was also shown that the neutral buoyant vehicles are more effective at small enough values of the Froude number. In particular, an airship could be more effective than a slow airplane (such as Solar Impulse 2). The theoretical estimations of the critical Reynolds number showed that the laminar vehicles and animal bodies are possible. The high efficiency of such shapes allows explaining the flight of pterosaurs.

Since the most effective vehicles must have very slender hulls and very elongated wings, further investigation must be focused on the problems of their strength and the stability in order to withstand heavy longitudinal and transverse forces and to avoid buckling.

List of literature

1.   http://www.extremetech.com/extreme/188752-chinas-supersonic-submarine-which-could-gofrom-shanghai-to-san-francisco-in-100-minutes-creeps-ever-closer-to-reality

2.   http://www.clubit.tv/2014/12/worlds-smallest-rc-drone-nano-quad-copter-2

3.   *Nesteruk I.* Rigid bodies without boundary-layer separation // Int. J. Fluid Mech. Res. − 2014. − **41**. − P. 260−281. doi: 10.1615/ InterJFluidMechRes.v41.i3.50

4.   *Nesteruk I., Passoni G., Redaelli A.* Shape of aquatic animals and their swimming efficiency // J. Marine Biology. − 2014. − Article ID 470715. doi: 10.1155/2014/470715

5.   *Savchenko Yu.N.* Perspectives of the supercavitation flow applications // Int. Conf. SuperFAST'2008, July 2−4, 2008, St. Petersburg, Russia.

6.   *Nesteruk I.* Drag drop on high-speed supercavitating vehicles and supersonic submarines // Прикладна гідромеханіка. − 2015. − **17**, № 4. − С. 52−57. − http://hydromech.org.ua/content/pdf/ph/ph-17-4%2852-57%29.pdf

7.   *Hoerner S.F.* Fluid-dynamic drag. − N.J.: Midland Park, 1965. − 416 p.

8.   *Loitsyanskiy L.G.* Mechanics of Liquids and Gases. − 6th ed. − New York and Wallingford: Begell House, 1995. − 961 p.

9.   *Garabedian P.R.* Calculation of axially symmetric cavities and jets // Pac. J. Math. − 1956. − **6**, № 4. − P. 611−684.

10.   *Нестерук І.Г.* Розрахунок опору тонких конусів з використанням другого наближення для форми утворених ними каверн // Прикладна гідромеханіка. − 2003. − **5 (77)**, № 1. − С. 42−46.

11.   *Nesteruk I.* Drag effectiveness of supercavitating underwater hulls // Supercavitation / I. Nesteruk, Ed. − Springer, 2012. − P. 79−106.

12.   *Nesteruk I.* On the shape of a slender axisymmetric cavity in a ponderable liquid // Fluid Dynamics. − 1979. − **14**, № 6. − P. 923−927. doi: 10.1007/BF01052000

13.   *Nesteruk I.* Some problems of axisymmetric cavitation flows // Fluid Dynamics. − 1982. − **17**, № 1. − P. 21−27. doi: 10.1007/BF01090694

14.   *Nesteruk I.* Influence of the flow unsteadiness, compressibility and capillarity on long axisymmetric cavities // 5th Int. Symposium on Cavitation, 2003, Osaka, Japan.

15.   *Gabrielly Y., von Karman Th.* What price speed // Mech. Eng. − 1950. − **72**, № 10. − P. 775−779.

16.   *Saibene F., Minetti A.E.* Biomechanical and physiological aspects of legged locomotion in humans // Eur. J. Appl. Physiol. − 2003. − **88**. − P. 297−316. doi: 10.1007/s00421-002-0654-9

17.   *Nesteruk I.* Reserves of the hydrodynamical drag reduction for axisymmetric bodies // Bulletin of Kiev University. Ser. Physics & Mathematics. − 2002. − № 1. − P. 112−118.

18.   *Seifert A., Greenblatt D., Wygnanski I.J.* Active separation control: an overview of Reynolds and Mach numbers effects // Aerosp. Sci. Technol. − 2004. − **8**. − P. 569−582. doi: 10.1016/j.ast.2004.06.007

19.   *Goldschmied F.R.* Integrated hull design, boundary layer control and propulsion of submerged bodies: Wind tunnel verification // Proc. AIAA/SAE/ASME 18th Joint Propulsion Conf., 1982. − P. 3−18.

20.   *Choi K.-S., Jukes T. N., Whalley R.* Turbulent boundary-layer control with plasma actuators // Phil. Trans. Royal Soc. − 2011. − **369**. − P. 1443−1458. doi: 10.1098/rsta.2010.0362

21.   *Landau L. D., Lifshits E. M.* Fluid Mechanics. − 2nd ed. − Butterworth-Heinemann, 1987. − Vol. 6. Course of Theoretical Physics. − 552 p.

22.   *Нестерук І.Г.* Особливості турбулізації та відриву примежового шару на тонких осесиметричних дозвукових тілах // Наукові вісті НТУУ "КПІ". − 2002. − № 3. − С. 70−76.

23.   *Buraga O.A., Nesteruk I., Savchenko Yu.N.* Comparison of slender axisymmetric body drag under unseparated and supercavitational flow regimes // Int. J. Fluid Mech. Res. − 2006. − **33**, № 3. − P. 255−264. doi: 10.1615/InterJFluidMechRes.v33.i3.40

24.   *Нестерук І.Г.* Часткова кавітація на видовжених тілах // Прикладна гідромеханіка. − 2004. − **6 (78)**, № 3. − С. 64−75.

25.   *Lorant M.* Investigation into high-speed of underwater craft // Nautical Magazine. − 1968. − **200**, № 5. − P. 273−276.

26.   *Sprott J.C.* Energetics of walking and running. − http://sprott.physics.wisc.edu/technote/walkrun.htm

27.   http://www.speedofanimals.com/animals/bottlenose_dolphin

28.   https://en.wikipedia.org/wiki/Automobile_drag_coefficient

29.   https://en.wikipedia.org/wiki/Eco-Runner_Team_Delft

30.   https://en.wikipedia.org/wiki/Aptera_2_Series

31.   https://en.wikipedia.org/wiki/Formula_One_car

32.   https://en.wikipedia.org/wiki/Antonov_An-225_Mriya

33.   https://en.wikipedia.org/wiki/Lift-to-drag_ratio

34.   https://en.wikipedia.org/wiki/Solar_Impulse

35.   https://en.wikipedia.org/wiki/Underwater_glider

36.   https://en.wikipedia.org/wiki/Hybrid_Air_Vehicles_HAV_304_Airlander_10

37.   https://www.sciencedaily.com/releases/2009/05/090507194511.htm

38.   http://animals.nationalgeographic.com/animals/birds/albatross/

39.   https://en.wikipedia.org/wiki/Albatross

40.   *Templin R.J., Chatterjee S.* Posture, locomotion, and paleoecology of pterosaurs. − Boulder, Colorado: Geological Society of America. − 2004. − P. 56−60.

41.   https://en.wikipedia.org/wiki/VA-111_Shkval

42.   https://en.wikipedia.org/wiki/Spearfish_torpedo

43.   http://www.wow.com/wiki/Mark_48_torpedo

References

1. *China's Supersonic Submarine, which could go from Shanghai to San Francisco in 100 Minutes, Creeps ever Closer to Reality* [Online]. Available: http://www.extremetech.com/extreme/188752-chinas-supersonic-submarine-which-could-gofrom-shanghai-to-san-francisco-in-100-minutes-creeps-ever-closer-to-reality

2. *Worlds Smallest RC Drone Nano Quad Copter* [Online]. Available: http://www.clubit.tv/2014/12/worlds-smallest-rc-drone-nano-quad-copter-2/

3. I. Nesteruk, "Rigid bodies without boundary-layer separation", *Int. J. Fluid Mech. Res.*, vol. 41, no. 3, pp. 260−281, 2014. doi: 10.1615/InterJFluidMechRes.v41.i3.50

4. I. Nesteruk *et al.*, "Shape of aquatic animals and their swimming efficiency", *J. Marine Biology*, article ID 470715, 2014. doi: 10.1155/2014/470715

5. Yu.N. Savchenko, "Perspectives of the supercavitation flow applications", in *Proc. Int. Conf. Superfast Marine Vehicles Moving Above, Under and in Water Surface (SuperFAST'2008)*, 2−4 July 2008, St. Petersburg, Russia.

6. I. Nesteruk, "Drag drop on high-speed supercavitating vehicles and supersonic submarines", *Applied Hydromechnics*, vol. 17, no. 4, pp. 52−57, 2015. Available: http://hydromech.org.ua/content/pdf/ph/ph-17-4%2852-57%29.pdf

7. S.F. Hoerner, *Fluid-Dynamic Drag.* Midland Park, N.J, 1965.

8. L.G. Loitsyanskiy, *Mechanics of Liquids and Gases,* 6th ed. New York, Wallingford: Begell House, 1995.

9. P.R. Garabedian, "Calculation of axially symmetric cavities and jets", *Pac. J. Math.*, vol. 6, no. 4, pp. 611−684, 1956.

10. I. Nesteruk, "Drag calculation for slender cones using the second approximation for created by them cavities", *Applied Hydromechanics*, vol. 5, no. 1, pp. 42−46, 2003 (in Ukrainian).

11. I. Nesteruk, "Drag effectiveness of supercavitating underwater hulls", in *Supercavitation*, I. Nesteruk, Ed. Springer, 2012, pp. 79−106.

12. I. Nesteruk, "On the shape of a slender axisymmetric cavity in a ponderable liquid", *Fluid Dynamics*, vol. 14, no. 6, pp. 923−927, 1979. doi: 10.1007/BF01052000

13. I. Nesteruk, "Some problems of axisymmetric cavitation flows", *Fluid Dynamics*, vol. 17, no. 1, pp. 21−27, 1982. doi: 10.1007/BF01090694

14. I. Nesteruk, "Influence of the flow unsteadiness, compressibility and capillarity on long axisymmetric cavities", in *Proc. 5th Int. Symposium on Cavitation (Cav2003)*, Osaka, Japan, 2003.

15. Y. Gabrielly and Th. von Karman, "What price speed?", *Mechanical Eng.*, vol. 72, no. 10, pp. 775−779, 1950.

16. F. Saibene and A.E. Minetti, "Biomechanical and physiological aspects of legged locomotion in humans", Eur. J. Appl. Physiol., vol. 88, pp. 297−316, 2003. doi: 10.1007/s00421-002-0654-9

17. I. Nesteruk, "Reserves of the hydrodynamical drag reduction for axisymmetric bodies", *Bulletin of Kiev University. Ser. Physics & Mathematics*, no.1, pp. 112−118, 2002.

18. A. Seifert *et al.*, "Active separation control: an overview of Reynolds and Mach numbers effects", *Aerosp. Sci. Technol.*, vol. 8, pp. 569−582, 2004. doi: 10.1016/j.ast.2004.06.007

19. F.R. Goldschmied, "Integrated hull design, boundary layer control and propulsion of submerged bodies: Wind tunnel verification", in *Proc. AIAA/SAE/ASME 18th Joint Propulsion Conf.*, pp. 3−18, 1982.

20. K.-S. Choi *et al.*, "Turbulent boundary-layer control with plasma actuators", *Phil. Trans. Royal Soc.*, vol. 369, pp. 1443−1458, 2011. doi: 10.1098/rsta.2010.0362

21. L.D. Landau and E.M. Lifshits, *Fluid Mechanics*, 2nd ed., vol. 6, *Course of Theoretical Physics.* Butterworth-Heinemann, 1987.

22. I. Nesteruk, "Peculiarities of turbulization and separation of boundary-layer on slender axisymmetric subsonic bodies", *Naukovi Visti NTUU KPI*, no. 3, pp. 70−76, 2002 (in Ukrainian).

23. O.A. Buraga *et al.*, "Comparison of slender axisymmetric body drag under unseparated and supercavitational flow regimes", *Int. J. Fluid Mech. Res.* vol. 33, no. 3, pp. 255−264, 2006. doi: 10.1615/InterJFluidMechRes.v33.i3.40

24. I. Nesteruk, "Partial cavitation on long bodies", *Applied Hydromechanics*, vol. 6, no. 3, pp. 64−75, 2004 (in Ukrainian).

25. M. Lorant, "Investigation into high-speed of underwater craft", *Nautical Magazine*, vol. 200, no. 5, pp. 273−276, 1968.

26. J.C. Sprott. *Energetics of Walking and Running* [Online]. Available: http://sprott.physics.wisc.edu/technote/walkrun.htm

27. *Bottlenose Dolphin Tursiops Truncatus* [Online]. Available: http://www.speedofanimals.com/animals/bottlenose_dolphin

28. *Automobile Drag Coefficient* [Online]. Available: https://en.wikipedia.org/wiki/Automobile_drag_coefficient

29. *Eco-Runner Team Delft* [Online]. Available: https://en.wikipedia.org/wiki/Eco-Runner_Team_Delft

30. *Aptera 2 Series* [Online]. Available: https://en.wikipedia.org/wiki/Aptera_2_Series

31. *Formula One Car* [Online]. Available: https://en.wikipedia.org/wiki/Formula_One_car

32. *Antonov An-225 Mriya* [Online]. Available: https://en.wikipedia.org/wiki/Antonov_An-225_Mriya

33. *Lift-to-Drag Ratio* [Online]. Available: https://en.wikipedia.org/wiki/Lift-to-drag_ratio

34. *Solar Impulse* [Online]. Available: https://en.wikipedia.org/wiki/Solar_Impulse

35. *Underwater Glider* [Online]. Available: https://en.wikipedia.org/wiki/Underwater_glider
36. *Hybrid Air Vehicles HAV 304 Airlander 10* [Online]. Available: https://en.wikipedia.org/wiki/Hybrid_Air_Vehicles_ HAV_304_ Airlander_10
37. *Flight of The Bumble Bee is Based More on Brute Force than Aerodynamic Efficiency* [Online]. Available: https://www.sciencedaily.com/releases/2009/05/090507194511.htm
38. *Albatross* [Online]. Available: http://animals.nationalgeographic.com/animals/birds/albatross/
39. *Albatross* [Online]. Available: https://en.wikipedia.org/wiki/Albatross
40. R.J. Templin and S. Chatterjee, *Posture, locomotion, and paleoecology of pterosaurs*. Boulder, Colorado: Geological Society of America, 2004, pp. 56−60.
41. *VA-111 Shkval* [Online]. Available: https://en.wikipedia.org/wiki/VA-111_Shkval
42. *Spearfish Torpedo* [Online]. Available: https://en.wikipedia.org/wiki/Spearfish_torpedo
43. *Mark 48 Torpedo* [Online]. Available: http://www.wow.com/wiki/Mark_48_torpedo

І.Г. Нестерук

ЕФЕКТИВНІСТЬ СТАЛОГО РУХУ ТА ЇЇ ВДОСКОНАЛЕННЯ З ВИКОРИСТАННЯМ БЕЗВІДРИВНОГО ТА СУПЕРКАВІТА-ЦІЙНОГО РЕЖИМІВ ОБТІКАННЯ

Проблематика. Ефективність сталого дозвукового руху транспортних засобів і тварин у повітрі та воді оцінюється за допомогою різних коефіцієнтів опору, співвідношень опір–вага та потужність–вага.

Мета дослідження. Вдосконалення вказаних характеристик із використанням спеціальних форм корпусів та крил, що усувають відрив примежового шару, та з використанням суперкавітаційного режиму обтікання для високошвидкісного руху у воді.

Методика реалізації. Аналітичні та числові оцінки з використанням відомих результатів для обтікання тонкого безвідривного тіла обертання й аеродинамічного профілю та для сталого суперкавітаційного режиму обтікання.

Результати дослідження. Отримано прості аналітичні формули для ефективності руху, критичних чисел Рейнольдса ламінарно-турбулентного переходу тощо і застосовано їх для різних наземних, водних та повітряних транспортних засобів, тварин і спортивної активності людей. У досить широкому діапазоні чисел Рейнольдса $10^6 \le \mathrm{Re}_V \le 10^8$ використання безвідривних форм дає істотне зниження опору порівняно зі звичними тілами обертання. У воді при $\mathrm{Re}_V > 10^7$ переваги має суперкавітаційний режим обтікання.

Висновки. Зазначене зниження опору відкриває перспективи проектування різних типів дуже ефективних повітряних та високошвидкісних підводних транспортних засобів.

Ключові слова: безвідривні форми; зменшення опору; ламінарно-турбулентний перехід; суперкавітація; співвідношення опір–вага; співвідношення потужність–вага.

И.Г. Нестерук

ЭФФЕКТИВНОСТЬ УСТАНОВИВШЕГОСЯ ДВИЖЕНИЯ И ЕЕ СОВЕРШЕНСТВОВАНИЕ С ИСПОЛЬЗОВАНИЕМ БЕЗ-ОТРЫВНОГО И СУПЕРКАВИТАЦИОННОГО РЕЖИМОВ ОБТЕКАНИЯ

Проблематика. Эффективность устойчивого дозвукового движения транспортных средств и животных в воздухе и воде оценивается с помощью различных коэффициентов сопротивления, соотношений сопротивление–вес и мощность–вес.

Цель исследования. Совершенствование указанных характеристик с использованием специальных форм корпусов и крыльев, которые устраняют отрыв пограничного слоя, и с использованием суперкавитационного режима обтекания для высокоскоростного движения в воде.

Методика реализации. Аналитические и численные оценки с использованием известных результатов для обтекания тонкого безотрывного тела вращения и аэродинамического профиля и для установившегося суперкавитационного режима обтекания.

Результаты исследования. Получены простые аналитические формулы для эффективности движения, критических чисел Рейнольдса ламинарно-турбулентного перехода и т.д., и применены для различных наземных, водных и воздушных транспортных средств, животных и спортивной активности людей. В достаточно широком диапазоне чисел Рейнольдса $10^6 \le \mathrm{Re}_V \le 10^8$ использование безотрывных форм дает существенное снижение сопротивления по сравнению с обычными телами вращения. В воде при $\mathrm{Re}_V > 10^7$ преимущества имеет суперкавитационный режим обтекания.

Выводы. Данное снижение сопротивления открывает перспективы проектирования различных типов очень эффективных воздушных и высокоскоростных подводных транспортных средств.

Ключевые слова: безотрывные формы; уменьшение сопротивления; ламинарно-турбулентный переход; суперкавитация; соотношение сопротивление–вес; соотношение мощность–вес.